Soft Matter

Ion Channels in Sulfonated Copolymer-Grafted Nanoparticles in Ionic Liquid

Journal:	*Soft Matter*
Manuscript ID	SM-ART-06-2022-000725.R1
Article Type:	Paper
Date Submitted by the Author:	23-Jun-2022
Complete List of Authors:	Li, Ruhao; Stevens Institute of Technology, Chemical Engineering & Materials Science Han, Yuke; Stevens Institute of Technology, Chemical Engineering and Materials Science Akcora, Pinar; Stevens Institute of Technology, Chemical Engineering and Materials Science

Ion Channels in Sulfonated Copolymer-Grafted Nanoparticles in Ionic Liquid

Ruhao Li, Yuke Han and Pinar Akcora

Department of Chemical Engineering and Materials Science, Stevens Institute of Technology

Hoboken, NJ 07030 USA

ABSTRACT

The use of ionic liquids as solvent for polymers or polymer-grafted nanoparticles provides an exciting feature to explore electrolyte-polymer interaction. 1-hexyl-3-methylimidazolium bis(trifluoromethylsulfonyl)imide (HMIm-TFSI) holds specific interactions with the polymer through ion-dipole or hydrogen bonding. For this work, poly(methyl methacrylate)-***b***-poly(styrene sulfonate) (PMMA-***b***-PSS) copolymer-grafted Fe_3O_4 nanoparticles with different sulfonation levels (~4.9-10.9 mol% SS) were synthesized and their concentration dependent ionic conductivities were reported in acetonitrile and HMIm-TFSI/acetonitrile mixture. We found that conductivity enhancement with the particle concentration in acetonitrile was due to the aggregation of grafted particles, hence sulfonic domain connectivity. The ionic conductivity was found to be related to the effective hopping transfer within ionic channels. To the contrary, the conductivity decreased or remained constant with increasing particle concentration in HMIm-TFSI/acetonitrile. This result was attributed to the ion coupling between ionic liquid and copolymer domains.

INTRODUCTION

Room temperature ionic liquids (RTILs) have low melting point yet maintain extremely low vapor pressure and non-volatility. RTILs have high ion density and conductivity and are used as electrolytes for energy storage devices[1-3], actuators[4-8] and nanoparticle stabilizers[9-11]. By mixing ILs with non-ionic diblock copolymers, solvation and specific interactions between polymer and IL can be utilized to enhance the ionic conductivity[12-14]. Further, copolymer morphologies and ionic mobility of ILs within hydrophilic phases of copolymer have been investigated to understand these hybrid materials[15, 16]. Interface and domain orientation were found to influence the ion transport in imidazolium-based IL incorporated poly(methyl methacrylate) (PMMA)-***b***-polystyrene (PS) diblock copolymer system[16].

We have worked on 1-hexyl-3-methylimidazolium bis(trifluoromethylsulfonyl)imide (HMIm-TFSI) incorporated PMMA-grafted nanoparticles in our previous studies[12-14, 17]. Different particle aggregation states were found to influence the dynamics of imidazolium cations[14], which was measured by quasi-elastic neutron scattering experiments. This was

possible as the incoherent scattering signal was coming mostly from the $HMIm^+$ and the PMMA chains were deuterated and $TFSI^-$ anions contain no hydrogen. The ion-pair disassociation effect due to ion-dipole interactions between methyl groups of PMMA and $TFSI^-$ anions of HMIm-TFSI resulted in increasing the number of free $HMIm^+$ cations and the ionic conductivity[13]. It was also measured that the long-range unrestricted diffusion of $HMIm^+$ cations was enhanced in the well-dispersed grafted nanoparticles compared to the neat IL[14, 18]. The preferential interaction between PMMA and $TFSI^-$ anions also contributed to the solvation of IL with the addition of solvents. Solvents with high dipole moments such as acetonitrile, acetone and methanol exhibited high ionic conductivity when mixed with IL. Acetonitrile, with the highest polarity among several solvents tested, showed the highest conductivity when equal masses of acetonitrile and IL were mixed[17]. Thus, the complex solvation that is induced by ion-dipole interactions between PMMA-IL influences the overall ion mobility and ionic conductivity of IL/solvent mixture containing PMMA-grafted nanoparticles[12, 14, 17].

In block copolymers of PMMA-***b***-poly(styrene sulfonate) (PSS) mixed with HMIm-TFSI, additional interactions between PSS and $HMIm^+$ by Coulombic forces co-exist with the solvated IL through interactions between PMMA and $TFSI^-$ [14, 19]. We have found that PMMA-***b***-PSS-grafted nanoparticles with low sulfonation amount (0.1 mol% SS) and long PMMA chains (398 kDa) exhibited the highest conductivity in acetonitrile and HMIm-TFSI mixtures compared to the particles with the higher sulfonation amount (3 mol%) and the shorter PMMA chains (123 kDa)[13]. The high conductivity of the low sulfonated sample was explained by the asymmetric counterion distributions of IL, where a higher portion of $TFSI^-$ anions interacted with the long PMMA chains. The ion-polymer coupling in both copolymer domains facilitates the disassociation of IL. TOA-protected SS groups and possible coupling of SS groups with $HMIm^+$ cations enhance the solubility of particles in HMIm-TFSI.

For this work, we prepared copolymers with various sulfonate amounts to further understand the solvation and interactions of the HMIm-TFSI with the PMMA-***b***-PSS copolymer. These interactions can result in aggregated strings or networks of strings as copolymer composition and particle concentration are varied. Furthermore, the aggregation of ionic clusters can be constrained via disassociation of IL with the preferential interactions of each counterion with the copolymer domains. Here, we report the aggregation of copolymer-grafted nanoparticles at a moderately wide range of sulfonation levels (4.86-10.82 mol% SS). The IL which is associated with the chains differently in various copolymer compositions is examined using impedance spectroscopy and the measured ionic conductivities are analyzed by percolation theory. Our results show that percolation of sulfonated domains in particle-based ion conductors is essential to foster conductivity in particle-based ion conductors.

EXPERIMENTAL SECTION

Preparation of Particles. Fe_3O_4 nanoparticles (NPs) were prepared via solvothermal reduction of iron (III) acetylacetonate [$Fe(acac)_3$] by 1,2-tetradecanodiol as reducing agent[20]. Oleic acid and oleylamine are surfactants that cease the growth and ripening of Fe_3O_4 grains during reaction and render the product compatibility in benzyl ether. Grafted NPs were drop-cast on Formvar grids for imaging. Fe_3O_4 NPs of 7-nm in diameter were imaged by transmission electron microscope (JEOL 2100 Plus S TEM) at 200 kV. Oleic acid and oleylamine on NPs were later replaced by the chain transfer agent, 4-cyano-4-(phenylcarbonothioylthio)pentanoic acid (CPDB). The anchoring of CPDB on Fe_3O_4 NPs is based on reported procedure[21] and was modified slightly with reduced CPDB amount and longer reaction time. Equal volume of 10 mg/mL Fe_3O_4/tetrahydrofuran (THF) and 20 mg/mL CPDB/THF were mixed to react for 72 h

with magnetic stirring. Particles were precipitated in cyclohexane and ethyl ether mixture by centrifuging at 4000 rpm for 15 min and redissolved in THF. CPDB anchoring on NPs is confirmed by Fourier transform infrared (FTIR, Bruker Optics Tensor 27) spectroscopy (**Figure S1**). The amount of CPDB is measured by thermogravimetric analyzer (Q50 TGA, TA Instruments).

SI-RAFT Polymerization of PMMA-*gr*-Fe_3O_4. PMMA chains were grown from CPDB-functionalized NPs by surface-initiated reversible addition-fragmentation chain-transfer (SI-RAFT) polymerization[22], by which the chain length and graft density can be controlled by monomer, initiator and CTA amounts (**Figure S2**). The grafting of PMMA is confirmed by FTIR (**Figure S3**) and the amount of surface ligands (CPDB and PMMA) and graft density were measured in TGA. Concentrated HCl was added to the PMMA-grafted nanoparticle solution (10 mg/mL in 5 mL THF) to etch the Fe_3O_4 NPs and the mixture solution was sonicated till the solution became clear. Methanol was later added, and the mixture was centrifuged at 6000 rpm for 10 min. The precipitated PMMA chains were dried in vacuum at room temperature to remove methanol, THF, HCl, and water. Finally, the product was redissolved in toluene. The weight-averaged molecular masses of grafted PMMA chains were measured using a gel permeation chromatography-light scattering (GPC/LS) device after etching the particles.

The GPC/LS system in our laboratory is equipped with a VARIAN PL 5.0μm Mixed–C gel column (7.5-mm ID), a light scattering detector (miniDawn, Wyatt Technology) and a refractive index (RI) detector (Optilab rEX, Wyatt). Averaged molecular masses of synthesized PMMA were measured as 67 kDa (Đ: 1.45) and 122 kDa (Đ: 1.53). Grafting density (GD) was determined through TGA with the equation:

$$\mathrm{GD} = \frac{m_{\mathrm{polymer}} N_{\mathrm{A}} \rho R}{m_{\mathrm{NP}} \quad 3\overline{M}_{\mathrm{w}}} \#(1)$$

m_{polymer} and m_{NP} are the mass of grafted chains and particle cores, respectively. N_{A} is the Avogadro constant; ρ is the particle density; R is the radius of iron oxide nanoparticles; $\overline{M}_{\text{w}}$ is the weight-averaged molecular weight of grafted chains.

Preparation of trioctylammonium *p*-styrenesulfonate (SS–TOA). Trioctylammonium (TOA) capping was necessary to produce hydrophobic SS-TOA monomer. TOA capped *p*-styrenesulfonate (SS-TOA) was prepared following the published procedure[23, 24]. TOA protection solubilized the copolymer-grafted particles in toluene.

Synthesis of PMMA-*b*-PSSTOA-grafted Nanoparticles. SS monomer was sequentially added to the living PMMA chains. The CTA, initiator, and monomer amounts used to synthesize the sulfonated copolymer particles are given in **Table S2**.

Hydrodynamic sizes of grafted particles before and after sulfonation were measured in dynamic light scattering (DLS, Zetasizer NanoS, Malvern). PSS amounts were determined by end-group analysis using ^{1}H NMR (Varian-400 spectrometer). The chemical shift was recorded in unit of parts per million (ppm) and was calibrated by $CDCl_3$ at 7.26 ppm.

Electrochemical Impedance Spectroscopy (EIS). The SP-300 electrochemical impedance spectrometer, Bio-Logic Science Instruments is used for EIS measurements. Samples were tested in a home-made liquid cell with stainless steel electrodes. The Nyquist plots, frequency-dependent conductivity and ionic conductivity were acquired by AC with 10 mV amplitude at the 7 MHz–1 Hz frequency range. The Nyquist plot was fitted by equivalent circuit (EC) with the ZView software. The frequency dependence of bulk conductivity is plotted in **Figure S4**. Ionic conductivities (σ') were obtained from the high-frequency plateau, where ionic mobility dominates the impedance spectra[25]. The bulk conductivity $\sigma'(\omega)$ was calculated per

the following equation 2[12].

$$\sigma'(\omega) = \frac{Z'}{k\left[(Z')^2 + (Z'')^2\right]} \#(2)$$

wherein ω is the angular frequency; Z' and Z'' are the real and imaginary parts of impedance; k is the cell constant which was determined using 0.01 M KCl standard (Ricca Chemical, 1412 μS/cm at 25 °C).

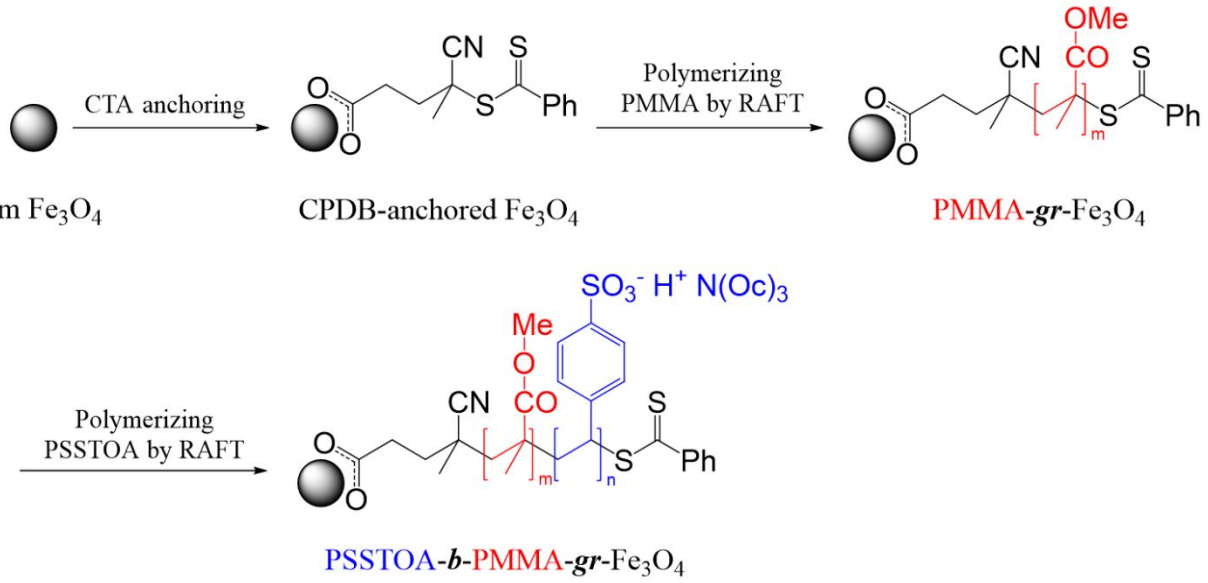

Figure 1 | Synthesis of PSSTOA-***b***-PMMA-grafted Fe_3O_4 nanoparticles by RAFT.

RESULTS AND DISCUSSION

We have synthesized PMMA-grafted chains with 67 kDa (in Samples **1-3**) and used them to polymerize PSS chains at varying lengths at sulfonation levels between 6.05-10.82 mol% SS; and prepared another grafted Sample **4** with 122 kDa PMMA chains with 4.86 mol% SS.

Stoichiometric percentage of SS was calculated by

$$[\mathrm{SS}]\% = \frac{n_{\mathrm{SS}}}{n_{\mathrm{MMA}} + n_{\mathrm{SS}}} \times 100\% \ \#(3)$$

wherein n_{SS} and n_{MMA} are the molar amount of SS and MMA monomers in copolymer chain, respectively.

Sample characteristics of $\overline{M}_{\mathrm{w}}$, $\overline{\mathrm{DP}}_{\mathrm{w,\,PMMA}}/\overline{\mathrm{DP}}_{\mathrm{w,\,PSSTOA}}$ (m/n) are given in **Table 1**. The molar ratio of blocks (m/n) varies between 8.3 and 19.7. Samples **1-3** are at lower graft density (GD: 0.15 chains/nm^2), and Sample **4** has GD: 0.69 chains/nm^2. GD values are much larger than the $1/R_{\mathrm{g}}^2$ of 67 kDa and 122 kDa PMMA chains, indicating the high graft density of chains around particles.

^{1}H NMR is used to calculate the sulfonation level (**Figure 2c**). Peaks at 7.2 ppm and 3.6 ppm are originated from the aromatic *ortho*-hydrogen on PSSTOA block and methyl hydrogen on PMMA block, respectively. The ratio of integrated areas ($A_{\mathrm{PSSTOA}}/A_{\mathrm{PMMA}}$) for the PSSTOA and PMMA is directly proportional to the number of hydrogens ($N_{\mathrm{H,\,SSTOA}}$, $N_{\mathrm{H,\,MMA}}$) per monomer, as stated in the following equation:

$$\frac{A_{\mathrm{PSSTOA}}}{A_{\mathrm{PMMA}}} = \frac{n_{\mathrm{SS}} N_{\mathrm{H,\,SSTOA}}}{n_{\mathrm{MMA}} N_{\mathrm{H,\,MMA}}} \#(4)$$

The integrated areas of all samples calculated prior to the intensity normalization are listed in **Table S1**.

Table 1 | Characteristics of PMMA$_m$-***b***-PSSTOA$_n$ grafted Fe_3O_4 nanoparticles.

Sample	$\overline{M}_{\mathrm{w,\,PMMA}}$ (kDa)	$\overline{\mathrm{DP}}_{\mathrm{w,\,PMMA}}$ (m)	Đ	GD (chains/nm^2)	SS% (mol%)	$\overline{\mathrm{DP}}_{\mathrm{w,\,PSSTOA}}$ (n)	m/n
1	67.0	669	1.45	0.15	6.05	43	15.6

2	67.0	669	1.45	0.15	9.42	70	9.6
3	67.0	669	1.45	0.15	10.82	81	8.3
4	122	1219	1.53	0.69	4.86	62	19.7

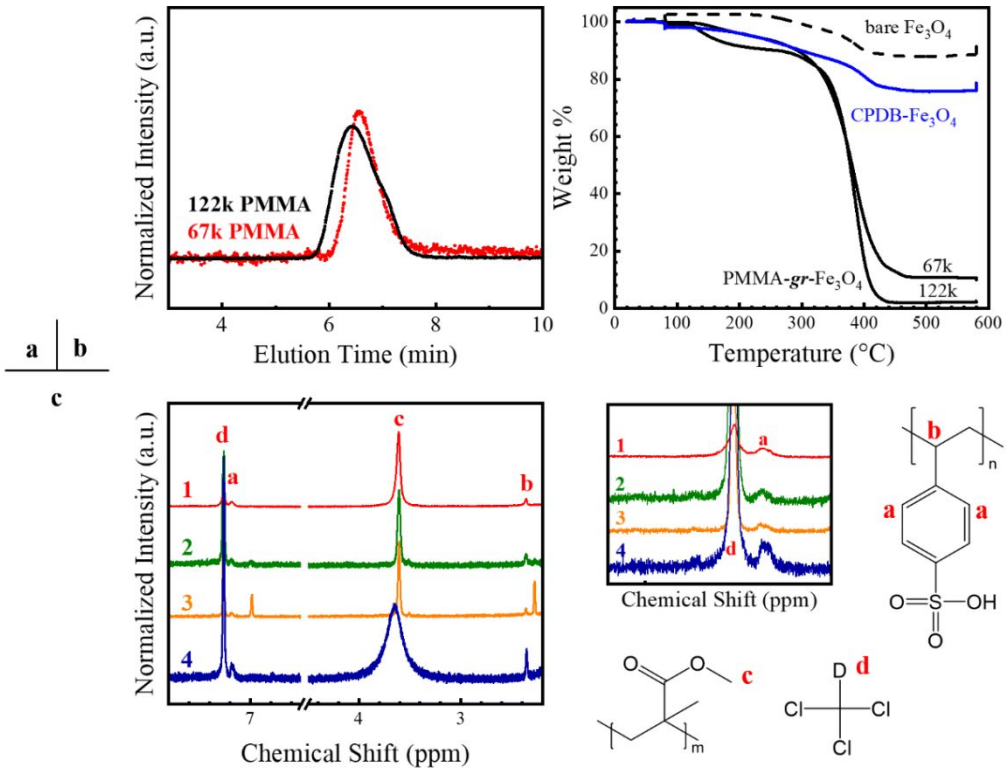

Figure 2 | **(a)** GPC-LS traces of 67 kDa and 122 kDa PMMA. **(b)** TGA data of the PMMA-grafted, the bare and CPDB-anchored Fe_3O_4. **(c)** ^{1}H NMR spectra of PMMA-***b***-PSSTOA copolymers (Samples 1-4).

All sulfonated samples have larger hydrodynamic sizes than their homopolymer precursors as shown in **Figure 3a**. Within Samples **1-3**, the hydrodynamic size increased from 100 nm to 225 nm as SS% is changed from 6.05 to 10.82 (**Figure 3b)**. In Sample **4**, the high GD provides stronger steric repulsion and particles have lower hydrodynamic sizes than Samples **1-3**. TEM data show aggregated structures at all sulfonation levels. Samples were solution cast from

toluene on grids. Sample **3** with the highest sulfonation amount showed the highly aggregated structures (**Figure 3c**). Good dispersion in Sample **4** is not surprising due to its strong steric repulsion of high GD chains.

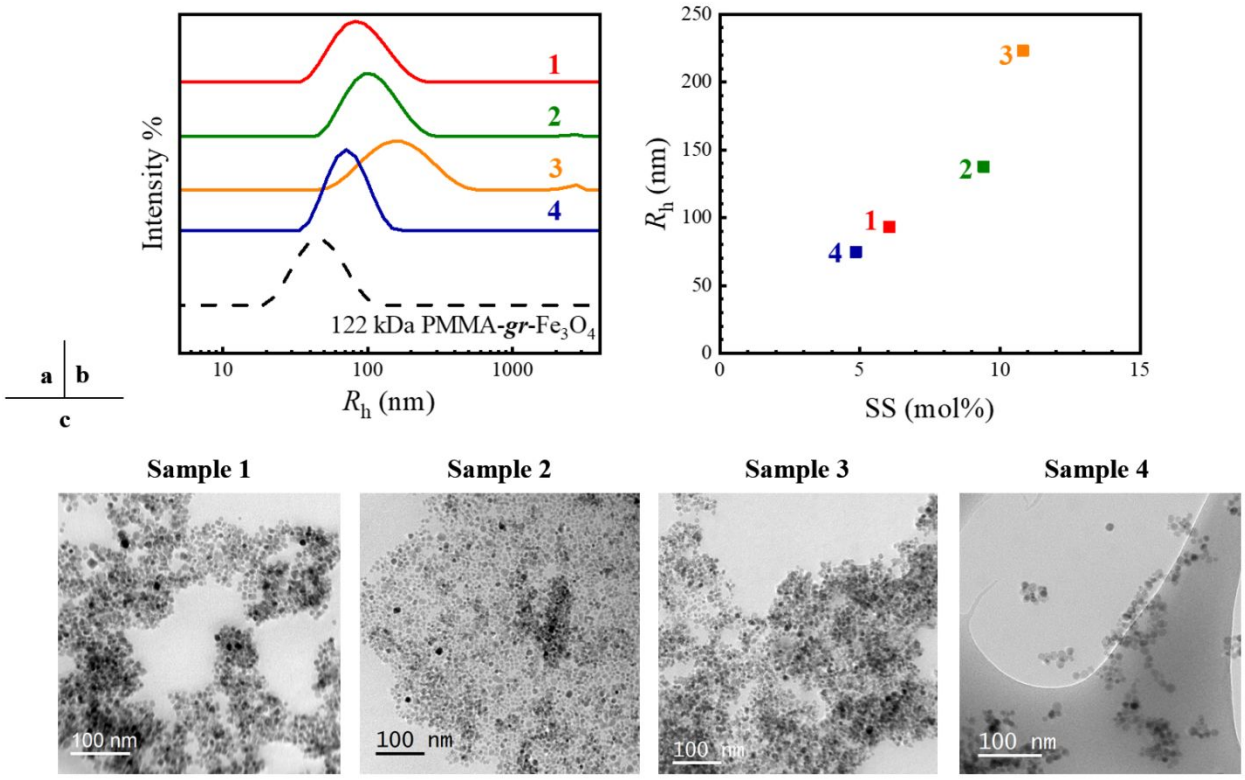

Figure 3 | **(a)** Z-averaged hydrodynamic size R_h distributions of all samples in toluene. **(b)** R_h of samples with varying SS mol% in toluene. **(c)** TEM data of PMMA-***b***-PSS grafted NPs.

The distribution of $TFSI^-$ anions around grafted particle aggregates are visualized in Scanning electron microscopy (SEM) and energy dispersive X-ray spectroscopy (EDS) (**Figure 4**). The Fe mapping easily locates the Fe_3O_4 NP cores. The dense Fluoride (F) signal on the Fe_3O_4 shows the $TFSI^-$ anion distribution because $TFSI^-$ is the only molecule containing F. The S signals on the other hand are denser in the outer regions of Fe_3O_4 and they are attributed to PSS. The N signal matches to the S mapping, revealing that it is from the $HMIm^+$. This matching between N and S signifies the affinity between $HMIm^+$ cations and PSS block. While these results are

qualitative, it helps us to demonstrate the preferential interactions between cations and PSS; as well as between anions and PMMA.

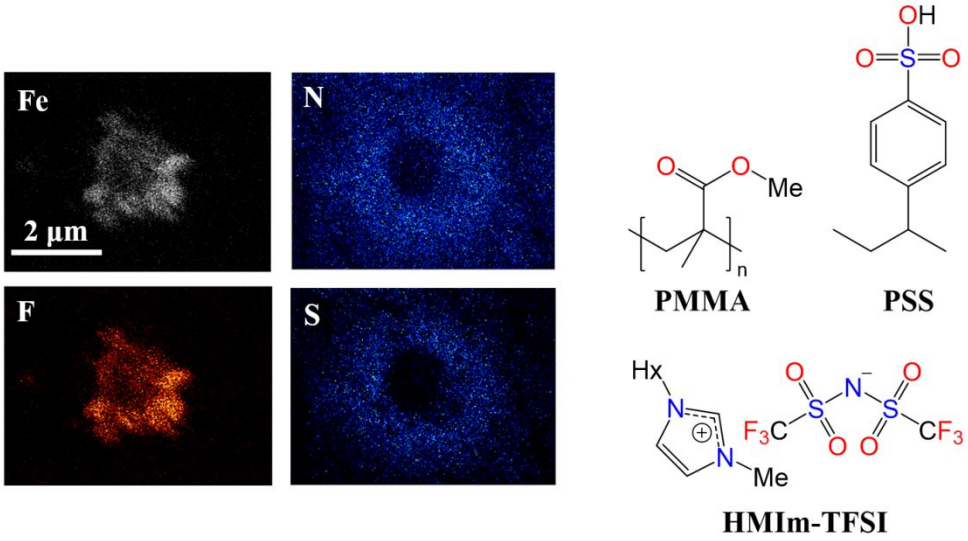

Figure 4 | SEM-EDS data of PMMA-***b***-PSS copolymer-grafted Fe_3O_4 NPs for Fe, F, N and S element mappings, and the chemical structures of species of interest.

Copolymer Samples **1-4** in acetonitrile at different concentrations were tested in EIS for conductive properties. The Nyquist plot shows the impedance in a complex plane. The shape of a typical Nyquist plot of an electrolyte solution contains Warburg impedance at lower frequency region, and single or multiple arcs at higher frequencies. The Warburg impedance is originated by the diffusion of ions and appears linear[26]. The arcs are attributed to both resistive and capacitive behavior, which can be further explained by ion transfer, dielectric constant at electrode-electrolyte interface[27]. Ionic conductivity (σ') is averaged from the AC frequency-dependent bulk conductivity in plateau region and the latter is calculated from the Nyquist plot via equation 2. **Figure 5** shows the ionic conductivity dependence on volume

fraction of PSS. Sample **4** with high GD (0.69 chains/nm^2) has lower conductivity than the other samples in acetonitrile. Conductivity increased sharply at low concentrations and then reached to more-like plateau values. We thus estimated the percolation threshold (ϕ_c) to be 0.001%, suggesting the percolating structure occurs at slightly lower concentration than our experiment range. The apparent enhancement in conductivity values with the increasing sulfonation amount was seen at high concentrations. Polymer ($\phi_{polymer}$) and PSSTOA (ϕ_{SSTOA}) volume fractions are calculated using the equations:

$$\phi_{polymer} = \frac{Cw}{\rho_{PMMA}}, \qquad \phi_{NP} = \frac{C(1-w)}{\rho_{NP}} \#(5)$$

$$\phi_{SSTOA} = \phi_{NP} x \#(6)$$

C is the mass concentration of polymer-grafted nanoparticles and w is the weight loss fraction of polymer-grafted NPs; ρ_{PMMA} and ρ_{NP} are densities of PMMA and Fe_3O_4, respectively; x is the sulfonation molar fraction.

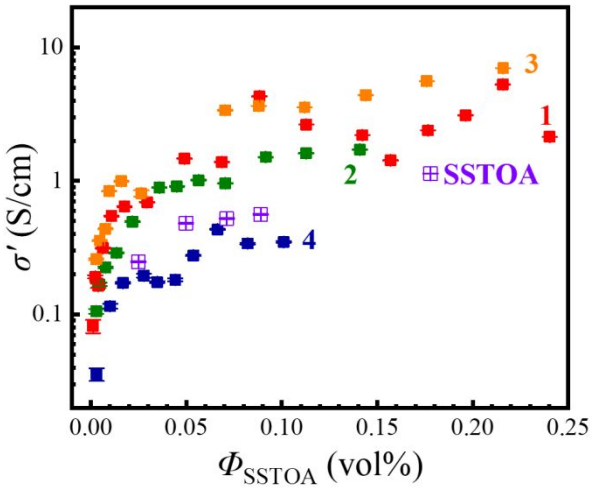

Figure 5 | Ionic conductivities (σ') of PMMA-***b***-PSS-grafted Fe_3O_4 NPs (Samples **1-4**) and

SSTOA monomer in acetonitrile with varying PSS volume fractions (ϕ_{SSTOA}).

We plotted the conductivity versus $\phi_{\mathrm{PGNP}} - \phi_{\mathrm{c}}$ and fit to a $\sigma' = \sigma_0(\phi_{\mathrm{PGNP}} - \phi_{\mathrm{c}})^t$ equation that describes the percolation model of the infinite-size network connectivity[28]. The linear fittings of the conductivity are ascribed to particle connectivity (**Figure 6a**). ϕ_{c} is the percolation threshold, and t is the critical exponent that depends on the connectivity of nanoparticles and is the slope of the linear fitting line. The geometric percolation threshold of hard spheres is reported to be 0.297[21]. The threshold ϕ_{c} depends on aspect ratio and can be low (0.001 vol%) for anisotropic nanofillers like carbon nanotube and carbon black[29-31]. The percolation threshold of our grafted particles is much lower than that of hard spheres as grafted particles have large hydrodynamic sizes (**Figure 3**). The interfacial stretching in PMMA-*b*-PSS[32] and the anisotropic self-assembly of particles[33, 34] are other ruling phenomena that govern the percolation of grafted particles. Another important factor is the electric percolation threshold occurring at the lower concentration than the mechanical percolation threshold as the ions hop between localized particle aggregates[30]. The exponent t is found to be around 0.6 in Samples **1-3** indicating a similarity to their network topologies (**Table S3**).

It is important to note the sharp increase of ionic conductivity was not seen for bare NPs and PMMA-grafted NPs (**Figure S5**). We compared the particle-grafted samples with the SSTOA monomer (**Figure 5**, purple open dots). In SSTOA, ions freely diffuse as there is no structure effect or ion coupling to the polymer. The ionic conductivity of SSTOA is expected to be higher than polymer-grafted NPs. However, the SSTOA was measured to be lower than all 3 samples. Thus, the high conductivity in low-GD Samples **1-3** was attributed to the percolating structures as illustrated in **Figure 6b**. The steric repulsion of high GD Sample **4** hinders entanglements between ionic groups of PSS. The relatively lower value of $t\,(0.542)$ signifies the lowest

connectivity, and the lowest value of R^2 represents a low explanatory power of percolation theory for this sample (**Table S3**). Interestingly, Sample **4** has the lower ionic conductivity than SSTOA monomer.

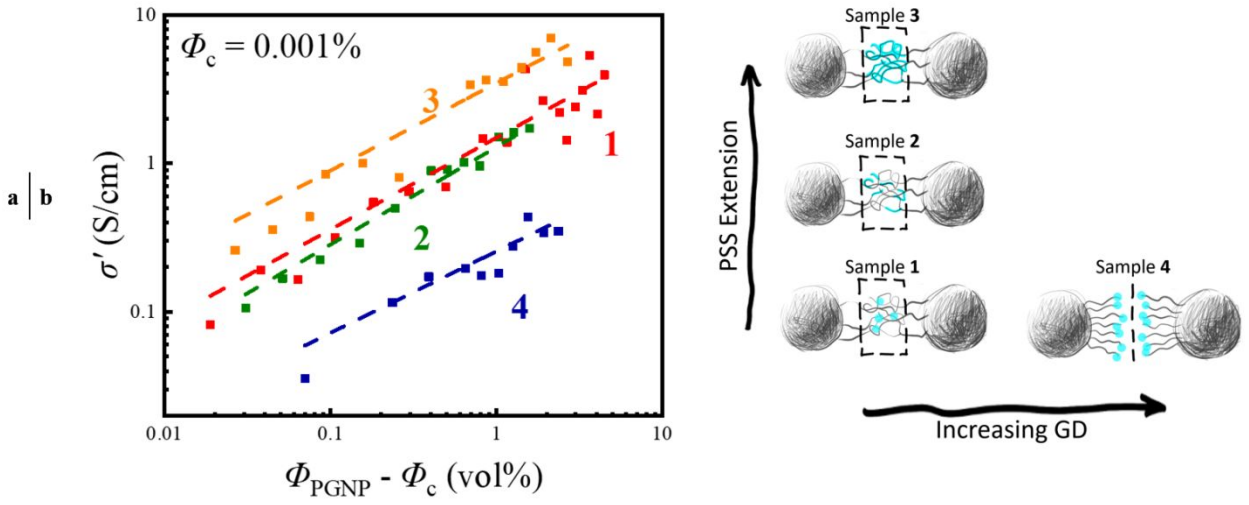

Figure 6 | **(a)** Ionic conductivity (σ') of PMMA-***b***-PSS copolymer-grafted NPs in acetonitrile as a function of the volume percentage, $\phi_{\mathrm{PGNP}} - \phi_{\mathrm{c}}$. **(b)** Schematic illustration of ionic connectivity between PMMA-***b***-PSS-grafted NPs for varying sulfonation amount in SS% (Samples **1-3**) and graft density (Samples **1** and **4**). The cyan parts refer to PSS blocks.

Furthermore, we used equivalent circuit (EC) models to analyze the impedance data of copolymer-grafted NPs in acetonitrile. Two EC models (**Figure S6**) numerically reproduce the Nyquist plots for the low and high conductivity range (**Figure S7**). Values of circuit elements (R_1, C_1 and CPE_1) are related to the polymer-grafted nanoparticle concentration. The R_1 element refers to the resistance of ions moving through the bulk electrolyte[35], and decreases with particle concentration (**Figure S8a**). Sample **3** has the strongest concentration dependence of R_1 value and Sample **4** has the weakest. The other elements (C_1 and CPE_1) refer to capacitance and increase with concentration in Samples **1-3** unlike Sample **4** (**Figure S8b-c**). The ion transport in

these Samples **1-3** enhances by the percolated sulfonated domains within the aggregated particles. Sample **4** does not exhibit this behavior because it does not form such effective networks. We note that the vehicular diffusion of free TOA^+ ions in acetonitrile has minor effect on the conductivity.

To the contrary, we observed that the conductivity of particles dispersed in HMIm-TFSI/acetonitrile decreased with concentration (**Figure 7a**). The coupling of PMMA with $TFSI^-$ and PSS with $HMIm^+$ reduces the free ion concentration, hence diffusion. Such interactions solvate the IL and aid in better dispersion in HMIm-TFSI (**Figure S9**) compared to that in acetonitrile as shown in Figure 3. Since both blocks of copolymer impair ion motion, increasing the polymer concentration (ϕ_{polymer}) lowers the free ion conductivity in Samples **1** and **4**. Samples **2** and **3** that can form network by their longer chain and lower graft density, ionic conductivities decrease only slightly. At very low concentration, Samples **1** and **3** have higher conductivity than the neat IL/acetonitrile. The decline of conductivity with particle concentration increase suggests that ion coupling of polymers becomes effective in Samples 1 and 3. The conductivity of ions that are coupled with PMMA and PSS balances out the high conductivity that is for the low particle concentration. The percolation is stronger in Sample **1** compared to Sample **4** and the large decrease in conductivity of Sample **4** was attributed to the weaker connectivity of PSS domains.

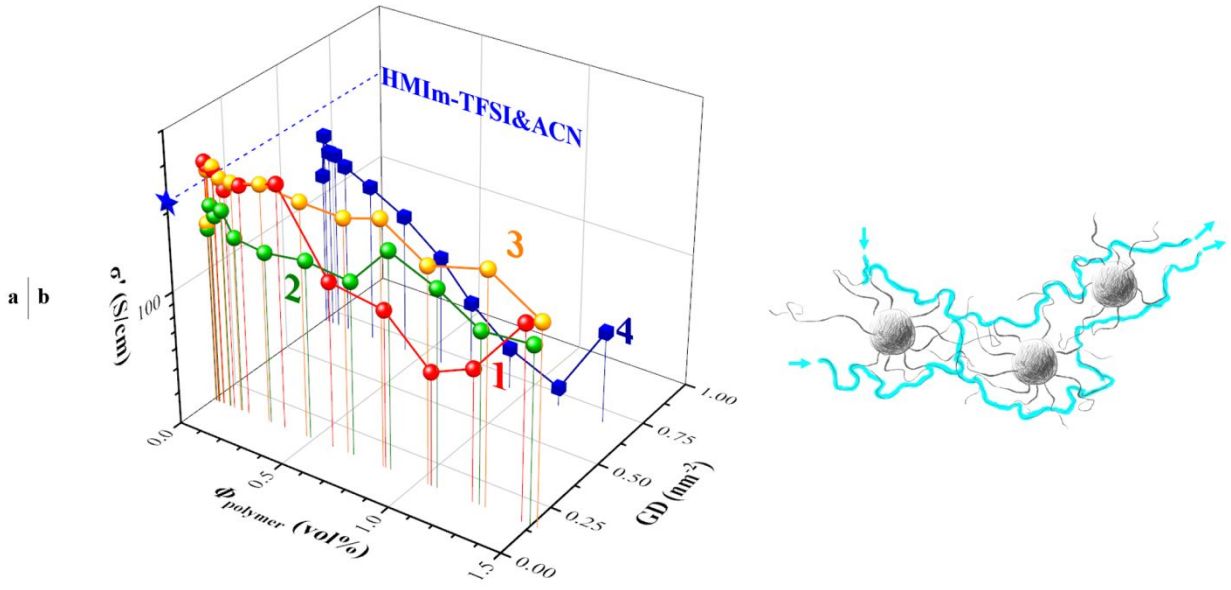

Figure 7 | **(a)** Ion conductivities of copolymer-grafted NPs in HMIm-TFSI/acetonitrile (ACN) for varying polymer concentration, $\phi_{polymer}$. Data point shown with star is for the neat HMIm-TFSI/ ACN. **(b)** Sulfonated chain percolation is represented with an illustrative work of aggregated grafted nanoparticles.

Conclusions

A series of PMMA-***b***-PSS copolymer-grafted Fe_3O_4 nanoparticles at varying sulfonation levels was prepared to study the macroscopic ionic conductivities of particles solvated in HMIm-TFSI. It is known that pure HMIm-TFSI conducts electricity through its ions diffusing in a vehicular mode. This work aims to understand how copolymer grafted NPs will interfere with the conductivity of HMIm-TFSI. SEM-EDS elemental mapping demonstrates the PMMA-$TFSI^-$ and PSS-$HMIm^+$ affinities. Here, we show that the network of polymer-grafted particles establishes *ion channels* where ions hop through the percolating sulfonated polymer in acetonitrile, that significantly enhances the ionic conductivity with concentration. The equivalent

circuit analysis of EIS data also supports that the percolating structures guide ion transport via hopping rather than free diffusion. Particles in HMIM-TFSI exhibited an opposite trend where conductivity decreased with grafted polymer concentration. The coupling of each polymer domain with the IL counterparts through ion-dipole interactions led to lower conductivity than that of neat IL. The low graft density and polymer interactions with the IL can enhance the dispersion state of polymer-grafted nanoparticles, however lower the transport of IL species. In conclusion, polymer-ion coupling and organization of sulfonated domains (in IL or solvent) both contribute to the ion transport in grafted-particle based electrolytes.

Conflicts of Interest

There are no conflicts to declare.

Acknowledgements

This work was supported by the National Science Foundation DMR Polymers program under award #1807802. We thank Dr. Tsengming Chou for his help with SEM-EDS experiments.

References

1. Chen, T.; Kong, W.; Zhang, Z.; Wang, L.; Hu, Y.; Zhu, G.; Chen, R.; Ma, L.; Yan, W.; Wang, Y.; Liu, J.; Jin, Z., Ionic liquid-immobilized polymer gel electrolyte with self-healing capability, high ionic conductivity and heat resistance for dendrite-free lithium metal batteries. *Nano Energy* **2018,** *54*, 17-25.

2. Koyilapu, R.; Singha, S.; Kutcherlapati, S. N. R.; Jana, T., Grafting of

vinylimidazolium-type poly(ionic liquid) on silica nanoparticle through RAFT polymerization for constructing nanocomposite based PEM. *Polymer* **2020,** *195*, 122458.

3. Beers, K. M.; Balsara, N. P., Design of Cluster-free Polymer Electrolyte Membranes and Implications on Proton Conductivity. *ACS Macro Letters* **2012,** *1* (10), 1155-1160.

4. Kim, O.; Shin, T. J.; Park, M. J., Fast low-voltage electroactive actuators using nanostructured polymer electrolytes. *Nature Communications* **2013,** *4* (1), 2208.

5. Kruusamäe, K.; Punning, A.; Aabloo, A.; Asaka, K., Self-Sensing Ionic Polymer Actuators: A Review. *Actuators* **2015,** *4* (1).

6. Kim, O.; Kim, H.; Choi, U. H.; Park, M. J., One-volt-driven superfast polymer actuators based on single-ion conductors. *Nature Communications* **2016,** *7* (1), 13576.

7. He, Q.; Vokoun, D.; Stalbaum, T.; Kim, K. J.; Fedorchenko, A. I.; Zhou, X.; Yu, M.; Dai, Z., Mechanoelectric transduction of ionic polymer-graphene composite sensor with ionic liquid as electrolyte. *Sensors and Actuators A: Physical* **2019,** *286*, 68-77.

8. Palmre, V.; Lust, E.; Jänes, A.; Koel, M.; Peikolainen, A.-L.; Torop, J.; Johanson, U.; Aabloo, A., Electroactive polymer actuators with carbon aerogel electrodes. *Journal of Materials Chemistry* **2011,** *21* (8), 2577-2583.

9. Men, Y.; Drechsler, M.; Yuan, J., Double-Stimuli-Responsive Spherical Polymer Brushes with a Poly(ionic liquid) Core and a Thermoresponsive Shell. *Macromolecular Rapid Communications* **2013,** *34* (21), 1721-1727.

10. Kerscher, B.; Appel, A.-K.; Thomann, R.; Mülhaupt, R., Treelike Polymeric Ionic Liquids Grafted onto Graphene Nanosheets. *Macromolecules* **2013,** *46* (11), 4395-4402.

11. Prabhu Charan, K. T.; Pothanagandhi, N.; Vijayakrishna, K.; Sivaramakrishna, A.; Mecerreyes, D.; Sreedhar, B., Poly(ionic liquids) as “smart” stabilizers for metal nanoparticles. *European Polymer Journal* **2014,** *60*, 114-122.

12. Liu, S.; Tyagi, M.; Akcora, P., Polymer-Coupled Local Dynamics Enhances Conductivity of Ionic Liquids. *Macromolecules* **2020,** *53* (15), 6538-6546.

13. Liu, S.; Wu, D.; Akcora, P., Ion-Containing Polymer-Grafted Nanoparticles in Ionic Liquids: Implications for Polymer Electrolyte Membranes. *ACS Applied Nano Materials* **2021,** *4* (8), 8108-8115.

14. Liu, S.; Liedel, C.; Tarakina, N. V.; Osti, N. C.; Akcora, P., Dynamics of ionic liquids in the presence of polymer-grafted nanoparticles. *Nanoscale* **2019,** *11* (42), 19832-19841.

15. Hoarfrost, M. L.; Tyagi, M. S.; Segalman, R. A.; Reimer, J. A., Effect of confinement on proton transport mechanisms in block copolymer/ionic liquid membranes. *Macromolecules* **2012,** *45* (7), 3112-3120.

16. Sharick, S.; Koski, J.; Riggleman, R. A.; Winey, K. I., Isolating the Effect of Molecular Weight on Ion Transport of Non-Ionic Diblock Copolymer/Ionic Liquid Mixtures. *Macromolecules* **2016,** *49* (6), 2245-2256.

17. Liu, S.; Walton, M.; Tarakina, N. V.; Akcora, P., Solvation in Ionic Liquids with Polymer-Grafted Nanoparticles. *The Journal of Physical Chemistry B* **2020,** *124* (23), 4843-4850.

18. Cai, M.; Yu, Q.; Liu, W.; Zhou, F., Ionic liquid lubricants: when chemistry meets tribology. *Chemical Society Reviews* **2020,** *49* (21), 7753-7818.

19. Yan, L.; Hoang, L.; Winey, K. I., Ionomers from Step-Growth Polymerization: Highly Ordered Ionic Aggregates and Ion Conduction. *Macromolecules* **2020,** *53* (5), 1777-1784.

20. Sun, S.; Zeng, H.; Robinson, D. B.; Raoux, S.; Rice, P. M.; Wang, S. X.; Li, G., Monodisperse MFe2O4 (M = Fe, Co, Mn) Nanoparticles. *Journal of the American Chemical Society* **2004,** *126* (1), 273-279.

21. Inoubli, R.; Dagréou, S.; Lapp, A.; Billon, L.; Peyrelasse, J., Nanostructure and

Mechanical Properties of Polybutylacrylate Filled with Grafted Silica Particles. *Langmuir* **2006,** *22* (15), 6683-6689.

22. Jiao, Y.; Akcora, P., Accelerated brush growth on nanoparticle surfaces by reversible addition-fragmentation chain transfer polymerization. *Journal of Polymer Science Part A: Polymer Chemistry* **2014,** *52* (12), 1700-1705.

23. Liu, Y.; Pollock, K. L.; Cavicchi, K. A., Synthesis of poly(trioctylammonium p-styrenesulfonate) homopolymers and block copolymers by RAFT polymerization. *Polymer* **2009,** *50* (26), 6212-6217.

24. Cavicchi, K. A., Synthesis and polymerization of substituted ammonium sulfonate monomers for advanced materials applications. *ACS Applied Materials and Interfaces* **2012,** *4* (2), 518-526.

25. Singh, M.; Odusanya, O.; Wilmes, G. M.; Eitouni, H. B.; Gomez, E. D.; Patel, A. J.; Chen, V. L.; Park, M. J.; Fragouli, P.; Iatrou, H.; Hadjichristidis, N.; Cookson, D.; Balsara, N. P., Effect of Molecular Weight on the Mechanical and Electrical Properties of Block Copolymer Electrolytes. *Macromolecules* **2007,** *40* (13), 4578-4585.

26. Mei, B.-A.; Munteshari, O.; Lau, J.; Dunn, B.; Pilon, L., Physical Interpretations of Nyquist Plots for EDLC Electrodes and Devices. *The Journal of Physical Chemistry C* **2018,** *122* (1), 194-206.

27. Ohno, H.; Fujita, K., Ionic Conductivity. In *Electrochemical Aspects of Ionic Liquids*, 2005; pp 75-81.

28. Ramasubramaniam, R.; Chen, J.; Liu, H., Homogeneous carbon nanotube/polymer composites for electrical applications. *Applied Physics Letters* **2003,** *83* (14), 2928-2930.

29. Yao, S.-H.; Dang, Z.-M.; Jiang, M.-J.; Xu, H.-P.; Bai, J., Influence of aspect ratio of carbon nanotube on percolation threshold in ferroelectric polymer nanocomposite. *Applied*

Physics Letters **2007,** *91* (21), 212901.

30. Richards, J. J.; Hipp, J. B.; Riley, J. K.; Wagner, N. J.; Butler, P. D., Clustering and Percolation in Suspensions of Carbon Black. *Langmuir* **2017,** *33* (43), 12260-12266.

31. Li, J.; Ma, P. C.; Chow, W. S.; To, C. K.; Tang, B. Z.; Kim, J. K., Correlations between Percolation Threshold, Dispersion State, and Aspect Ratio of Carbon Nanotubes. *Advanced Functional Materials* **2007,** *17* (16), 3207-3215.

32. He, H.; Zhong, M.; Adzima, B.; Luebke, D.; Nulwala, H.; Matyjaszewski, K., A Simple and Universal Gel Permeation Chromatography Technique for Precise Molecular Weight Characterization of Well-Defined Poly(ionic liquid)s. *Journal of the American Chemical Society* **2013,** *135* (11), 4227-4230.

33. Wei, Q.-h.; Han, M.; Zhou, C.-h.; Ming, N.-b., Percolation of two-dimensional attractive coagulated particles. *Physical Review E* **1994,** *49* (5), 4167-4171.

34. Jiao, Y.; Akcora, P., Assembly of Polymer-Grafted Magnetic Nanoparticles in Polymer Melts. *Macromolecules* **2012,** *45* (8), 3463-3470.

35. Irvine, J. T. S.; Sinclair, D. C.; West, A. R., Electroceramics: Characterization by Impedance Spectroscopy. *Advanced Materials* **1990,** *2* (3), 132-138.